ACS APPLIED MATERIALS & INTERFACES

Research Article

Cite This: ACS Appl. Mater. Interfaces 2018, 10, 11486−11494

www.acsami.org

Spatial and Chemical Surface Guidance of NK Cell Cytotoxic Activity

Guillaume Le Saux,*[,†,‡] Avishay Edri,[§] Yossi Keydar,[†,‡] Uzi Hadad,[‡] Angel Porgador,[§] and Mark Schvartzman*[,†,‡]

[†]Department of Materials Engineering, [‡]Ilse Katz Institute for Nanoscale Science & Technology, and [§]The Shraga Segal Department of Microbiology, Immunology and Genetics, Faculty of Health Sciences, Ben Gurion University of the Negev, Beer Sheva 84105, Israel

Supporting Information

ABSTRACT: Studying how different signaling pathways spatially integrate in cells requires selective manipulation and control of different transmembrane ligand−receptor pairs at the same time. This work explores a novel method for precisely arranging two arbitrarily chosen ligands on a micron-scale two-dimensional pattern. The approach is based on lithographic patterning of Au and TiO_2 films, followed by their selective functionalization with Ni−nitrilotriacetic acid−histidine and biotin−avidin chemistries, respectively. The selectivity of chemical and biological functionalizations is demonstrated by X-ray photoelectron spectroscopy and immunofluorescence imaging, respectively. This approach is applied to produce the first type of bifunctional surfaces with controllably positioned ligands for activating the receptors of natural killer (NK) immune cells. NK cells were used as a model system to demonstrate the potency of the surface in guiding site-selective cell attachment and activation. Upon applying the suitable ligand or ligand combination, the surfaces guided the appropriate single- or bifunctional attachment and activation. These encouraging results demonstrate the effectiveness of the system as an experimental platform aimed at the comprehensive understanding of the immunological synapse. The great simplicity, modularity, and specificity of this approach make it applicable for a myriad of combinations of other biomolecules and applications, turning it into the "Swiss knife" of biointerfaces.

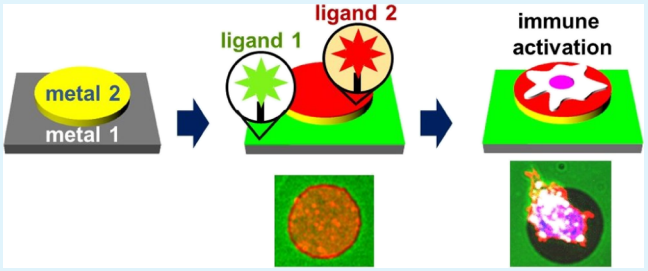

KEYWORDS: *heterogeneous surfaces, self-assembled monolayers, biofunctionalization, NK cells, immunological synapse*

INTRODUCTION

Cell signaling—a communication process that manages and directs cell function—is an extensively studied research field. A large variety of transmembrane proteins are involved in signaling in both directions, as well as in the cell adhesion to the extracellular matrix (ECM) and to other cells. Although each protein transduces its own specific signal upon recognition by its extracellular cognate ligand, the outcome of cell activity depends on the cumulative signals generated and transduced by various ligand−receptor pairs. For instance, signaling cross talk between integrin $\alpha_v\beta_3$ and vascular endothelial growth factor receptor-2 promotes neovascularization in endothelial cells.[1] Also, cell−ECM and cell−cell adhesion receptors produce a highly integrating signaling network that regulates cell polarity, migration, proliferation and survival, differentiation, morphogenesis, and tissue homeostasis.[2] Furthermore, because different ligand−receptor pairs participate in many pathways, their spatiotemporal colocalization is vital for regulating the cellular responses to the incoming signals.

One important biosystem in which many signaling pathways are integrated is the immunological synapse—a large and complex cluster of signaling receptors and their cognate ligands, which is formed at the interface between an immune cell and a target cell—for example, a virus-infected cell or a cancer cell. For the cytotoxic CD8+ T cell or the natural killer (NK) lymphocyte-type immune cell, the immunological synapse regulates its activation and cytotoxic activity through activating and inhibitory receptors, whose signaling balance determines whether a target cell will be tolerated or attacked. Thus, while each receptor has its own signaling properties,[3,4] the resulting function of a lymphocyte may depend on the integration of two or more signaling pathways.[5−8]

Not only is the presence of various ligand−receptor pairs recruited into the immunological synapse important for the immune function but also their spatiotemporal arrangement. In T cells, the TCR/CD3 complex was found to be activated upon its segregation from CD45.[9,10] CD3 also segregates from CD28, modulating the cross talk between the two proteins and affecting CD28 signaling because of the limited diffusion of Lck that phosphorylates CD28.[11,12] On the other hand, matching the sizes of the inhibitory ligand−receptor pair (HLA-C/KIR2DL1) and the activating ligand receptor pair (MICA/NKG2D)[13] appears necessary for their signaling integration in NK cells.[14] In NK cells, KIR2DL1 reorganizes at the nanometer

Received: December 26, 2017
Accepted: March 20, 2018
Published: March 20, 2018

DOI: 10.1021/acsami.7b19643
ACS Appl. Mater. Interfaces 2018, 10, 11486−11494

scale upon engagement with NKG2D.[15] Although these and many other types of activating−inhibitory signal integration have been observed and described during the last years, their spatiotemporal mechanism is still barely understood.

It should be noted that the importance of this mechanism is both fundamental and applied to all types of biointerface interactions including immunological synapses as well as interactions between other cell types including modified cell types for therapeutic purposes. Chimeric antigen receptor (CAR)-based immunotherapy is a rapidly emerging and extensively studied clinical approach with a remarkable potency against blood cancer.[16] Recently, the Food and Drug Administration approved a CD-19 CAR-specific immunotherapy against B-cell acute lymphoblastic leukemia.[17] Today, new methods of immunotherapies are extensively explored for other tumors.[18] In this context, the fundamental study of how different signals are integrated in the immunological synapse and cooperatively regulate its function is essential for the rational design of future immunotherapeutic approaches. Yet, such a study requires an experimental platform that enables simultaneous manipulation and segregation of different receptor−ligand pairs in a controlled and selective manner.

Spatial control of two or more receptor−ligand pairs is extremely challenging because it requires controllable positioning of different chemical functionalities within a micron or nanometer length scale. For instance, selective modification of bimetallic Au/TiO_2 surfaces was used for site-specific attachment of two different adhesion ligands; however, the fact that the two ligands had to be synthesized with specific functional groups for attaching to the metals makes this approach complex and inflexible.[19] Additionally, bifunctional surfaces were produced via sequential immobilization of two ligands onto photolithographically patterned microdomains via peptide linkage; however, this approach can only be applied to small synthetic peptides with one reactive amine moiety.[20] Therefore, there is still a need for a universal and versatile approach for the site-selective immobilization of multiple ligands of any kind onto the same surface.

In this work, being motivated by the modeling of the molecular and spatial diversity of the immunological synapse, we engineered two-dimensional (2D) bifunctional "smart" surfaces that allow selective and controlled manipulation and segregation of different immune ligands. Furthermore, we demonstrated the ability of these surfaces for the programmable guiding of the adhesion and activation of NK cells. Our bifunctional surface consists of lithographically patterned microdomains of Au and TiO_2, which are selectively biofunctionalized with two ligands. To achieve the functionalization selectivity, we combined, for the first time to the best of our knowledge, (i) Au−thiol[21] and (ii) TiO_2−phosphonic acid[22] chemistries with (iii) biotin−avidin[23] and (iv) nitrilotriacetic acid (NTA)−Ni−histidine[24] conjugations (Figure 1a−d). We demonstrated that the combination of avidin and Ni−NTA functionalities can be used for facile and robust site-selective biofunctionalization by different combinations of biotin- and His-conjugated ligands (Figure 1e−g). We verified the functionalization selectivity by X-ray photoelectron spectroscopy (XPS) and fluorescence spectroscopy. Furthermore, we demonstrated that by arbitrarily choosing the surface architecture and varying the chemical composition of our surfaces, we can spatially encode the interaction and the immune response of NK cells. Importantly, the previously demonstrated bifunctional substrates for cell recognition were

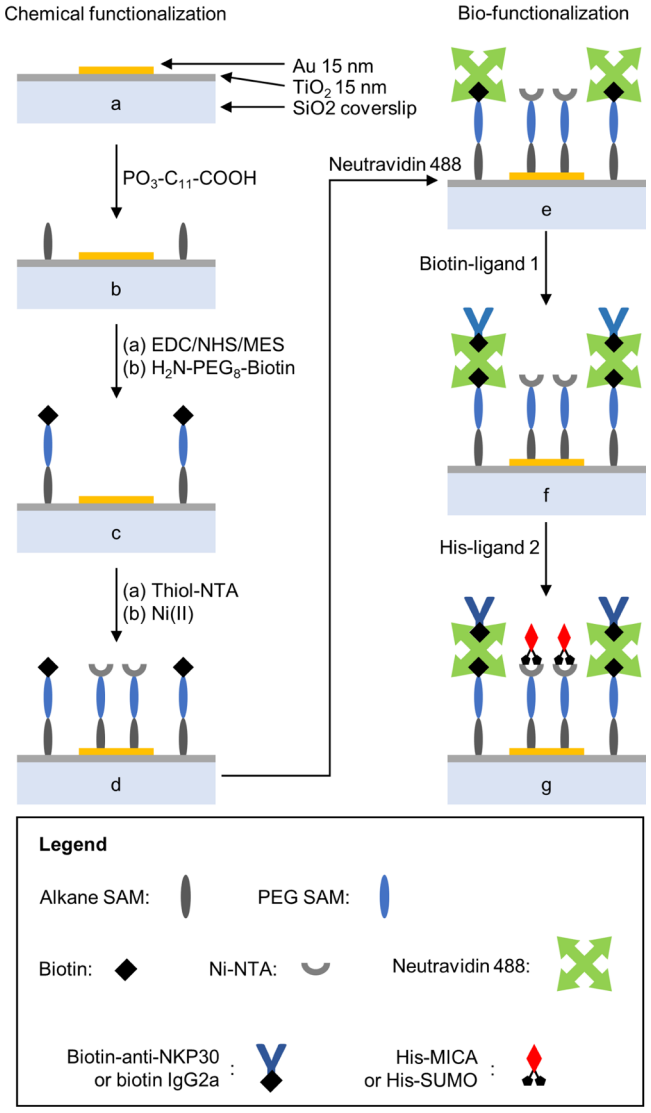

Figure 1. Chemical and bio-orthogonality. Sequential modification of TiO_2/Au mixed surfaces to obtain the surfaces presenting two distinct bioactive molecules. (a) Titanium and gold are evaporated on glass; patterns of gold disks on titanium are obtained via photolithography and selective etching of the exposed gold. (b) TiO_2 is modified with a carboxyl-terminated monolayer via phosphonic acid chemistry. (c) Poly(ethylene glycol) (PEG)−biotin is attached to TiO_2 through a peptide linkage. (d) Gold is derivatized with NTA-terminated monolayers via thiol chemistry, followed by the chelation of nickel, thus yielding Ni(ii)−NTA complexes. (e) Oregon Green 488 NeutrAvidin is linked to the biotin-terminated TiO_2. (f) Biotin-labeled anti-NKP30 or IgG2a is coupled to TiO_2 via NeutrAvidin. (g) Finally, histidine-tagged MICA or SUMO is attached to the gold disk through the Ni(ii)−NTA−histidine affinity.

based on the direct binding of specific ligands chemically synthesized for that purpose.[20,25−29] Here, we used biotin and His conjugations that are applicable to a myriad of proteins and peptides.[30] Therefore, although in this work we focused on certain NK cell ligands, our bifunctional approach is highly versatile and modular and can be applied to endless combinations of biofunctionalities.

DOI: 10.1021/acsami.7b19643
ACS Appl. Mater. Interfaces 2018, 10, 11486−11494

RESULTS AND DISCUSSION

Chemical functionalization of Au and TiO_2 in a selective fashion is at the *crux* of this work. To demonstrate that our bifunctional approach is chemically selective, we lithographically fabricated Au disks (10 μm in diameter) onto glass coverslips covered with thin films of TiO_2 and chemically functionalized them according to Figure 1a–d. Briefly, TiO_2 was functionalized with a carboxyl-terminated phosphonic acid, followed by coupling of the biotin linker via peptide chemistry. Au was then functionalized with thiolated NTA, followed by the immobilization of Ni by its chelation with NTA. For the details of fabrication and functionalization, see the Experimental Section.

We used XPS to analyze the outermost portion of a surface and, by using elements as specific markers for each type of substrate, estimated the degree of specificity of our functionalization method. Table 1 provides the changes in atomic proportions of the surface-modified Au and TiO_2.

Table 1. Experimental Atomic Composition (%) Obtained by XPS

atomic %	S	C	O	N	P	Ni
TiO_2	0.12	61.37	33.69	4.36	0.56	
Au	0.43	29.54	67.48	1.71		0.84

Figure 2 shows the chemical structure of the base layers on Au and TiO_2 and the associated high-resolution spectra of the N 1s, P 2p, and Ni 2p regions. High-resolution spectra for the C 1s, O 1s, and S 2p regions are also displayed in Figure S1. For

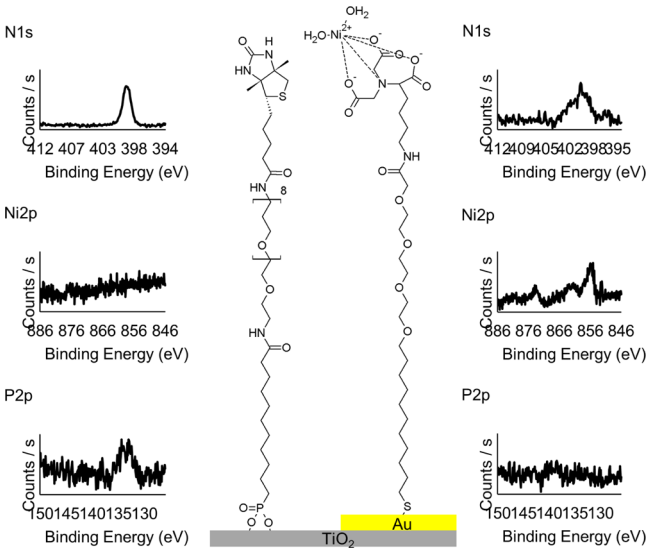

Figure 2. Orthogonal chemical functionalization: XPS analysis. Continuous layers of either gold or TiO_2 were chemically modified. Both substrate types underwent the same modification steps simultaneously. The base layer consisting of biotin-terminated TiO_2 and Ni(II)–NTA-modified gold was analyzed. This corresponds to surface 4 in Figure 1. Although both the monolayers have carbon, nitrogen, oxygen, and sulfur in common, the presence of nickel can only stem from the NTA moiety and phosphorus is only present in 11-phosphoundecanoic acid (PO_3–C_{11}–COOH). High-resolution scans of the N 1s, Ni 2p, and P 2p regions were taken on each metal, demonstrating the orthogonality of the method used to modify the bimetallic substrates.

TiO_2, grafting of PO_3–C_{11}–COOH is confirmed by the presence of a peak at 133–134 eV in the P 2p scan, which is close to the values obtained elsewhere on titanium[31] or other substrates.[32,33] After the activation of the carboxyl moieties, NH_2–PEG_8–biotin is coupled to TiO_2, which is demonstrated by the presence of a nitrogen peak stemming from the amide linkages as well as a peak in the S 2p region (see Figure S1). For Au, effective coupling of the Ni–NTA self-assembled monolayer (SAM) formation reagent is supported by the presence of a wide peak in the N 1s region as well as a clear peak for Ni 2p. Phosphorus is the ad hoc marker for the functionalization of TiO_2, while the Ni signal should stem from the Au-bound Ni–NTA only. As we performed all the functionalization steps on both Au and TiO_2 simultaneously, the absence of Ni on TiO_2, as well as the absence of P on Au, confirms that the functionalization of bimetallic substrates with the desired molecules is highly selective.

To demonstrate that we can further biofunctionalize our chemically functionalized surfaces in a selective manner, His-MICA was used as the ligand for the attachment to Ni–NTA. Au–TiO_2 patterns were fabricated and selectively functionalized with biotin and Ni–NTA as described previously. Then, NeutrAvidin Oregon 488 was coupled to the biotin-terminated TiO_2 background, and His-MICA was attached to the Ni–NTA-functionalized Au disks (Figure 3a). To verify that the His-MICA attachment was site-selective, mouse anti-MICA was coupled to the His-MICA-functionalized areas, followed by labeling with antimouse Alexa Fluor 555 and imaging the surface with a fluorescence microscope. It is clearly seen that Au disks are specifically stained, while the surrounding TiO_2 exhibits very little red fluorescence (Figure 3b). In addition, there is a significant signal contrast between Au disks and the NeutrAvidin Oregon Green 488-terminated TiO_2 (Figure 3c). Figure 3d shows the merged fluorescent signals, confirming the highly precise attachment of His-MICA to the Au disks. The presence of oligoethylene glycol units in the monolayer backbones (see the chemical composition of the base layers in Figure 2) ensures a high degree of orthogonality by limiting nonspecific protein adsorption. This result is also useful for the cell studies described below because it ensures specificity of interaction of the cell-surface receptors with the surface-bound ligands. Furthermore, TiO_2 can then be further functionalized using biotin-labeled proteins. As a proof of concept, we coupled Cy3–PEG–biotin to the NeutrAvidin-terminated TiO_2, while Au was functionalized with His-MICA but not labeled with Alexa Fluor 555. As seen previously, Oregon Green-labeled NeutrAvidin reveals the TiO_2 background, while the Au disks are darker (Figure S2a). Cy3–PEG–biotin was then coupled to the NeutrAvidin-modified TiO_2, as shown in Figure S2b. Colocalization of green and red (as seen from the yellow in Figure S2c) shows that the coverage for both NeutrAvidin and Cy3–PEG–biotin is homogeneous.

To demonstrate that our selective functionalization can be applied to the surface guiding of immune function in cells through controlled segregation of different ligands, we prepared bifunctional surfaces combining ligands to the activating receptors, such as the physiological ligand to the NKG2D-activating receptor (MICA)[34] or monoclonal antibody that activates the NKp30-activating receptor (anti-NKp30),[35] and mock ligands, such as murine IgG2a or SUMO, and studied the response of NK cells to these heterogeneous surfaces. We prepared three types of bifunctional surfaces that expressed spatially localized ligands for the NK cells: (i) MICA on Au and

DOI: 10.1021/acsami.7b19643
ACS Appl. Mater. Interfaces 2018, 10, 11486–11494

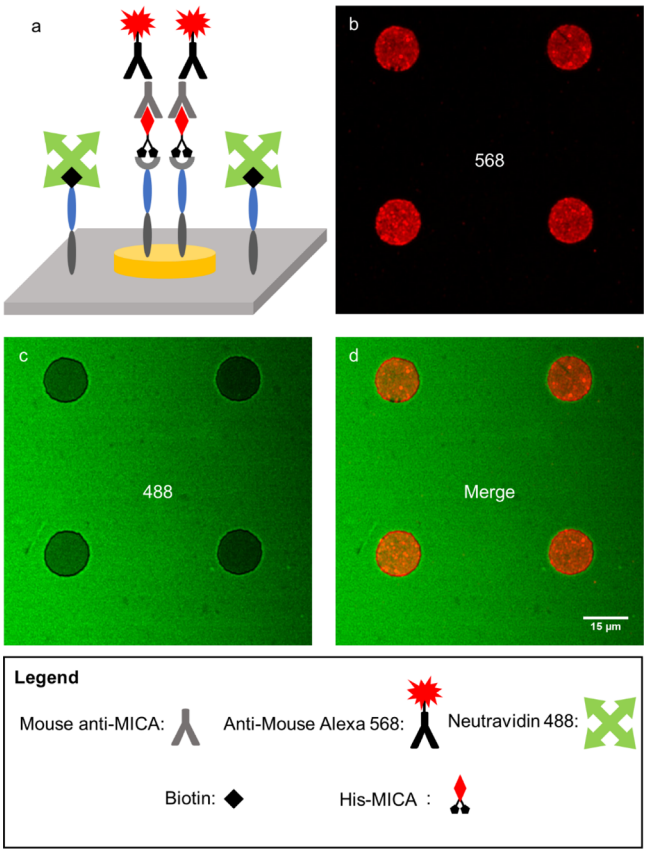

Figure 3. Orthogonal biofunctionalization of TiO_2/Au surfaces: characterization by fluorescence. (a) Schematic of the functionalized surface as imaged in panel d. (b) His-MICA was attached to the gold disks. Using immunofluorescence, mouse anti-MICA is then coupled to the MICA-terminated surface, followed by anti-mouse Alexa 568. (c) Oregon Green 488-labeled NeutrAvidin is coupled to the biotin-functionalized TiO_2. (d) Merging images (a) and (b) confirm the segregation of MICA to the gold disks only, whereas NeutrAvidin solely resides on TiO_2.

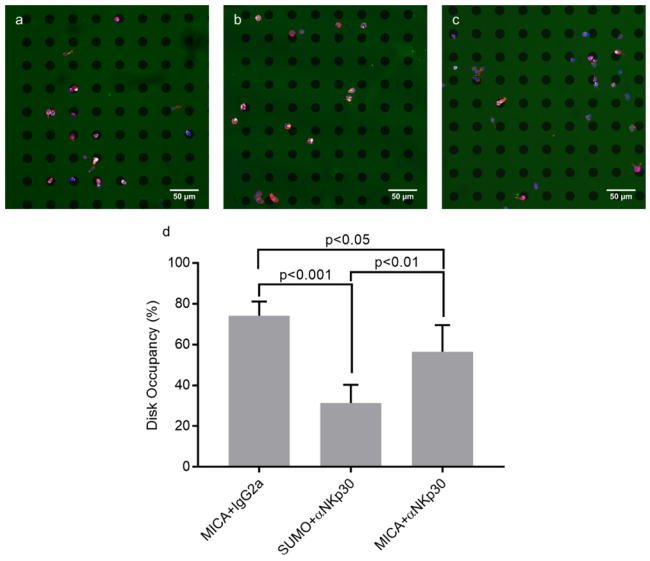

Figure 4. Cell adhesion. Primary NK (pNK) cells were seeded on the surfaces for 3−4 h in serum and IL-2 poor culture medium at 37 °C and 5% CO_2. The surface types were (a) His-MICA on gold and biotin−IgG2a on TiO_2, (b) His-SUMO on gold and biotin−anti-NKP30 on TiO_2, and (c) His-MICA on gold and biotin−anti-NKP30 on TiO_2. After fixation in 4% paraformaldehyde (PFA), the cells were permeabilized, blocked, and stained with Alexa Fluor 555 phalloidin to visualize the cytoskeleton and DAPI for the nuclei. (d) Disk occupancy was quantified, which reveals the guided adhesion of the NK cells to the gold disks modified with activating ligands when compared with mock proteins. Analysis of variance and Tukey's post hoc test were performed to assess the significant changes in behavior. The results were considered significant for $p < 0.05$. *P*-values are also reported for comparisons of interest.

murine IgG2a on TiO_2, (ii) SUMO on Au and anti-NKp30 on TiO_2, and (iii) MICA on Au and anti-NKp30 on TiO_2. Also, we prepared bifunctional surfaces for negative control, positioning IgG2a on TiO_2 and SUMO on Au. We seeded the NK cells onto the surfaces and incubated them for 3−4 h. We then rinsed the surfaces, fixed the remaining cells, and stained the actin cytoskeleton and nuclei with phalloidin and DAPI fluorescent tags, respectively (see the Experimental Section for details).

The representative images and quantification of disk occupancy are shown in Figure 4a−d. Here, disk occupancy is defined as the ratio of the cells adhered to the Au disks to the total number of cells per field. The expected disk occupancy for a bifunctional surface with no preferred affinity for a ligand is 50%. We found that on the surfaces of type (i), cells displayed a higher affinity for MICA-functionalized Au disks than for the IgG2a-coated background (Figure 4a), with a disk occupancy of ≈74% (Figure 4d). Conversely, for the surfaces of type (ii), in which the disks were functionalized with SUMO, the disk occupancy was around 30%, indicating a preferential cell affinity to the anti-NKp30-functionalized background (Figure 4b). This shift in behavior was found to be significantly different ($p < 0.001$). Finally, for the surfaces of type (iii), the disk occupancy seemed slightly in favor of MICA (56%), as illustrated in Figure 4c. However, Tukey's post hoc test revealed a significant difference in disk occupancy between type (i) and (iii) surfaces ($p < 0.05$). Were adhesion to have been more favored on MICA than on anti-NKp30, this would not have been the case. This result therefore indicates that cell affinity is not specific on surfaces presenting both MICA and anti-NKp30. The negative control consisting of pristine Au/TiO_2 surfaces or surfaces coated with IgG2a and SUMO showed poor affinity and specificity altogether (too few cells were present on the surfaces for an effective quantification; see Figure 5b for a representative image). The results were strikingly consistent throughout the repeated experiments.

It was previously demonstrated that the NK cells did not require adhesion molecules such as intercellular adhesion molecule to strongly interact with a ligand-coated surface, even though in low numbers (less than 100 cells per cm^2).[36] Furthermore, the surface density of the bioactive molecules on the system that was used for this study stands in the fmol/mm^2 range. Here, using a fluorescence-based method, we estimated the surface density of the bioactive molecules and obtained values in pmol/mm^2 for TiO_2 and in tens of fmol/mm^2 for the gold disks (see section S3 in the Supporting Information for experimental details). These values fall within the range previously mentioned, thus explaining why we could see the NK cells adhere to our surfaces. However, because NK cells are known for their motility,[37] we cannot exclude the fact that upon landing on the surfaces, NK cells may have migrated toward the regions of higher affinity, like gold with MICA or TiO_2 with anti-NKp30. This claim is downplayed by the fact that NKG2D

DOI: 10.1021/acsami.7b19643
ACS Appl. Mater. Interfaces 2018, 10, 11486−11494

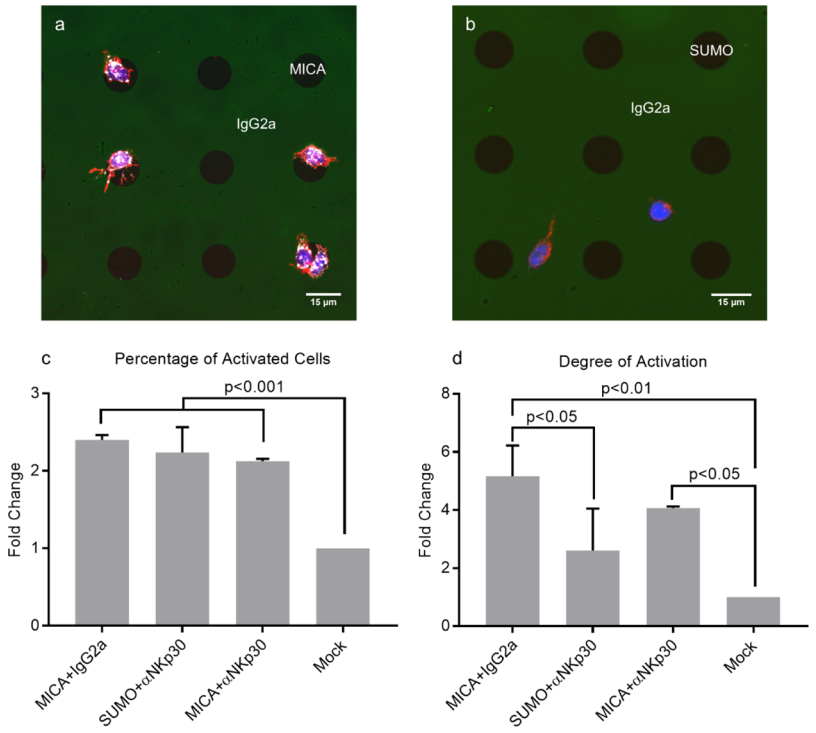

Figure 5. Cell activation. pNK cells were seeded as previously described. (a,b) Representative image of the NK cells stained with Alexa Fluor 555 phalloidin to visualize the cytoskeleton, DAPI for nuclei, and APC-labeled anti-CD107a as a marker for NK cell activation. In (a), the disks are functionalized with MICA and the titanium background with IgG2a. In (b), the disks are modified with SUMO and TiO_2 with IgG2a. (c) Percentage of activated NK cells on various regions of the substrates was quantified, which shows that more cells are activated on the substrates modified with activating ligands. (d) Degree of NK cell activation shows a two- to fivefold increase in the degree of activated NK cells on the surfaces presenting MICA or anti-NKp30 or both. Analysis of variance and Tukey's post hoc test were performed to assess the significant changes in behavior. The results were considered significant for $p < 0.05$. *P*-values are also reported for comparisons of interest.

is known to mediate the inhibition of the NK cell chemotaxis.[38] Furthermore, the surfaces produced here do not present the molecules that interact with the chemotactic receptors present on the NK cell membrane, which may thus not be sufficient to sustain the migration.[39] In contrast, we know that the cells were seeded on the surfaces at a density of roughly 170 000 per cm^2. From the images such as those shown in Figure 4, we calculate the number of cells per cm^2 equal to 20 000−30 000 cells for all surface types. Even though this value is 2 orders of magnitude higher than what was previously observed,[36] it still means that 80−90% of the seeded cells were lost during the experiment, most probably during the various washing steps involved afterward. We therefore hypothesize that although the seeded cells sedimented randomly onto our surfaces, only those with a firm enough grip remained. In our case, this firm grip stems from the interaction of the NK cells with either MICA or anti-NKp30, resulting in the cells being guided by the underlying pattern.

Interestingly, although the role of activating ligands is to induce the formation of an immunological synapse, here we demonstrated that their surface pattern can spatially guide the NK cells. Yet, such guiding is possible only in combination with a second ligand that would form a high contrast in terms of its cell affinity. Here, we showed that the mock ligands used in our experiments, which do not interact with the transmembrane proteins expressed on the cell surface, can form such a contrast. For instance, for the sample with MICA on Au disks and IgG2a on TiO_2 background, we observed the surface guidance to the disks (Figure 4a,d). Similarly, for the sample with SUMO on Au disks and anti-NKp30 on TiO_2, we observed the cell guidance toward the background. Yet, for the sample (iii) that combined MICA and the anti-NKp30 system—both are activating ligands—MICA-modified Au did not override TiO_2 presenting anti-NKp30 in terms of its cell affinity. This finding emphasizes that the difference in how various ligands interact with the transmembrane proteins is important for their combination for the surface guiding of cells.

We studied whether and how our bifunctional surface can guide not only the spatial positioning of the NK cells but also their immune function, through the imaging of CD107a that correlates with NK cell activation.[40] This correlation stems from the fact that the activated NK cells transport lytic granules to the immune synapse and fuse them to the membrane, causing their degranulation in a way that exposes CD107a molecules to the outer side of the membrane. Here, we detected the exposed CD107a using a fluorescently tagged monoclonal antibody, thus identifying events related to NK cell activation.

For activation assays, we used similar bifunctional surfaces and experimental conditions as described in the previous section, except that we incubated the cells with Allophycocyanin (APC)-labeled anti-CD107a. Importantly, after fixation, the cells were not permeabilized to prevent damage to their membrane and potential staining of the internal CD107a. A representative image of the NK cells on a surface with MICA disks and IgG2a background is shown in Figure 5a.

As seen previously, the cells interact more specifically with the MICA disks. Conversely, the cells adhered poorly to the surfaces presenting the mock proteins SUMO and murine IgG2a (Figure 5b). The degree of activation can be quantified

DOI: 10.1021/acsami.7b19643
ACS Appl. Mater. Interfaces 2018, 10, 11486−11494

by the fluorescence intensity of the APC anti-CD107a, which appears white in the images. We also performed *z*-stack imaging to locate the APC-tagged granules and cytoskeleton with regard to the surface. In Figure S4 (Supporting Information), we observe that for both the granules and cytoskeleton, the point of maximum intensity is closer to the surface than to the distal end of the cell. This result is in good agreement with the previous work which demonstrated that when the NK cells are activated, their cytoskeleton and lytic granules are polarized toward their target.[41]

The overall results of NK cell activation are shown in Figure 5c. Less than 40% of cells were found to be activated when lying over either IgG2a or SUMO. This amount of activation sharply contrasts with that found on activating substrates (i.e., MICA, anti-NKp30, or MICA + anti-NKp30), where more than 80% of the cells were activated ($p < 0.001$). The fact that the percentage of activated cells is similar for MICA and anti-NKp30 confirms that both the surface types stimulated cell activation in a similar fashion. We also assessed the average degree of activation per cell for the activated cells through the intensity of the APC anti-CD107 signal (Figure 5d). We observed that even when activated, the cells on the IgG2a- or SUMO-modified surfaces produced less anti-CD107 signal than those on MICA, anti-NKp30, or MICA/anti-NKp30 surfaces ($p < 0.01$). Interestingly, the degree of activation on anti-NKp30 was notably lower than that on MICA ($p < 0.05$). This implies that MICA may be more potent than anti-NKp30 in triggering NK cell degranulation and is further validated, given that per given area, there are 6−12 times more anti-NKp30 on TiO_2 than MICA on gold disks (see section S3 in the Supporting Information). However, it is, to our knowledge, not relevant to compare the potency of a ligand (i.e., MICA) with that of an antibody (anti-NKP30) as the mechanisms of interaction are different. Furthermore, the relative amount of NKG2D or NKp30 ligands expressed on the outer membrane of the NK cells varies between either donors or the NK cell subsets or even the organ of sampling,[42] thus making it arduous to unequivocally conclude on the relative potency of MICA compared with that of NKp30.

It should be noted that because of the small disk size, the NK cells never rest entirely on the disks and are often variably in contact with both the disks and the background. Conversely, because the background area is much larger than that of the disks, the cells on the background are often in contact with the background ligands only. Using this pattern, we were therefore able not only to decipher the individual effect of either MICA or anti-NKp30 but also to investigate their combined effect at the interface of the MICA/anti-NKp30 surfaces. In Figure 5 c, the percentage of activated cells on MICA/anti-NKp30 is equivalent to that on both MICA and anti-NKp30. Furthermore, while MICA triggered higher NK cell degranulation than anti-NKp30, the cells on both did not fare better (Figure 5d). This absence of synergy between the NKG2D and NKp30 receptors may arise from the ligands and antibodies being segregated on either Au or TiO_2. Therefore, costimulation may not have been ideal. Taken together, these results show that when two activating ligands are spatially segregated, there is no cumulative effect on the NK cell immune response.

CONCLUSIONS

Understanding the spatial cross talk between different signaling pathways in the immunological synapse requires a spatial control over different ligands. Such a control requires site-specific positioning of different ligands on the same surface, in a manner that controllably mimics the molecular composition of the APC membrane. Here, we demonstrated an innovative approach to produce bifunctional surfaces, on which two arbitrarily chosen ligands can be completely segregated and precisely arranged in a micron-scale 2D pattern. The surface modification process was based on the lithographic patterning of Au and TiO_2, followed by their selective chemical functionalization with thiol and phosphonic acid and further biofunctionalization via Ni−NTA−His and biotin−NeutrAvidin conjugations. Using XPS and fluorescent imaging, we verified that both chemical and biofunctionalization are highly selective. As a proof of concept, we used NK cells as a model system to demonstrate the ability of our bifunctional surfaces for the site-selective guiding and immunological activation of the cells. We showed that the NK cells have preferential affinity to both MICA and anti-human NKp30 ligands and that this affinity was leveled on surfaces presenting both activating biomolecules. In addition, we were able to guide NK cell activation toward MICA or anti-human NKp30. We observed that CD107a expression, which indicates the degree of degranulation in activated NK cells, was the highest on the MICA-modified areas but saw no cumulative effect between MICA and anti-NKp30. These encouraging results demonstrate the effectiveness of our system as an experimental platform aimed at the comprehensive understanding of the immunological synapse.

Surfaces with controlled ligand position aimed at mimicking the extracellular environment have been engineered using various functionalization approaches but mostly through controlled immobilization of one bioactive agent.[19,43−48] Here, we demonstrated selective bifunctional approach to mimic the molecular diversity of the extracellular environment, whose key advantages are its simplicity and modularity. After selective functionalization of a bimetallic pattern with Ni−NTA and NeutrAvidin, we can then proceed to the facile biofunctionalization of each metal with either histidine- or biotin-tagged biomolecules, respectively. The catalog of available proteins and antibodies tagged with histidine and biotin highlights that such a system could be used in endless applications that require bifunctional systems with controlled geometry.

EXPERIMENTAL SECTION

Chemicals. Analytical reagent grade acetone and absolute ethanol were purchased from BioLab Ltd. (Israel) and used as is. Elga PureLab Flex system was used to obtain ultrapure water. Au etchant standard, PO_3−C_{11}−COOH, NTA-terminal SAM formation reagent (thiol−NTA), *N*-(3-dimethylaminopropyl)-*N*′-ethylcarbodiimide hydrochloride (EDC), *N*-hydroxysuccinimide (NHS), 2-(*N*-morpholino)-ethanesulfonic acid (MES), *O*-(2-aminoethyl)-*O*′-[2-(biotinylamino)-ethyl]octaethylene glycol (NH_2−PEG_8−biotin), and nickel(II) chloride hexahydrate were all purchased from Sigma-Aldrich (Israel).

Reagents for Biofunctionalization. Dulbecco's phosphate-buffered saline (PBS), skim milk, and Tween20 were purchased from Sigma-Aldrich. NeutrAvidin Oregon Green 488-conjugated anti-mouse Alexa Fluor 555 was obtained from Life Technologies (Rhenium, Israel). Biotin anti-human CD337 (biotin anti-NKp30) was purchased from BioLegend (Enco, Israel). Biotinylated goat anti-mouse IgG2a human absorbed (biotin IgG2a) was obtained from Southern Biotech (Enco, Israel). Human MICA protein, His tag (His-MICA), and Small Ubiquitin-like Modifier, His tag (His-SUMO), were purchased from SinoBiological (China). CellGro SCGM medium was obtained from CellGenix. Il-2 (PeproTech) and heat-inactivated

DOI: 10.1021/acsami.7b19643
ACS Appl. Mater. Interfaces 2018, 10, 11486−11494

human AB plasma were obtained from healthy donors (SIGMA, male AB, H-4522), and PFA was purchased from Sigma-Aldrich. Mouse anti-MICA was purchased from R&D Systems (Biotest, Israel). Cy3−PEG−biotin was obtained from Nanocs (USA).

Fabrication of Patterned Au/TiO_2 Surfaces. Ti and Au (15 nm) were successively evaporated onto glass slides. The samples were then patterned with disk motifs by photolithography. Finally, Au was removed from the exposed regions by using an Au etchant. After rinsing the surfaces with water, the photoresist was then completely removed by sonicating the slides for 5 min in acetone. Each sample consists of 2.54 × 2.54 cm microscope slides. Each slide contains between 10 and 20 fields of Au/TiO_2 microarrays, each field being 1 mm^2 in size.

Selective Chemical Functionalization. First, TiO_2 was functionalized. Micropatterned slides were cleaned with ethanol and water and dried under a stream of nitrogen and baked at 120 °C for 5 min. After plasma cleaning, the slides were immediately immersed in a 5 mM aqueous solution of PO_3−C_{11}−COOH for 24 h. To facilitate dedissolution of PO_3−C_{11}−COOH in water, a catalytic amount of NaOH was also added. Upon complete reaction time, the samples were directly placed in an oven at 120 °C for 24 h without rinsing. The surfaces were then copiously rinsed with water and immersed for 1 h in an aqueous solution of EDC, NHS, and MES at the concentrations of 0.2, 0.1, and 0.1 M, respectively followed by rinsing with water. TiO_2 was then functionalized with biotin by overnight incubation in a 1 mM aqueous solution of NH_2−PEG_8−biotin. The samples were then copiously rinsed with water and ethanol. Au was functionalized by reacting overnight in a 0.2 mM ethanolic solution of thiol−NTA. After generous rinsing with ethanol and water, the samples were then incubated for 2 h in nickel(II) chloride, followed by rinsing in water. The chemical structure of the obtained surfaces is shown in Figure 2.

Selective Biofunctionalization. The samples were blocked for 30 min at 37 °C in PBS with 5% skim milk, followed by 30 min incubation in 25 μg/mL NeutrAvidin Oregon Green 488 in PBS with 5% skim milk at room temperature. The surfaces were rinsed 3 × 5 min in PBS with 0.1% Tween20. The samples were then immersed for 2 h at room temperature in a solution containing 12.5 μg/mL of either biotin anti-NKp30 or biotin IgG2a, in PBS with 5% skim milk, followed by rinsing 3 × 5 min in PBS with 0.1% Tween20. The surfaces were incubated overnight at 4 °C in either His-MICA or His-SUMO at a concentration of 2 μg/mL in PBS. Finally, the samples were rinsed 2 × 5 min in PBS with 0.1% Tween20 plus once with neat PBS and stored in PBS before being used for cell studies.

Primary NK Cell Purification. pNK cells were purified from peripheral blood of healthy, adult, volunteer donors, recruited by written informed consent, as approved by the Institutional Review Board Ben-Gurion University of the Negev (BGU). The cells were isolated using a human negative selection-based NK isolation kit (RosetteSep, Miltenyi Biotec). The purified NK cells were then cultured in a stem cell serum-free growth medium (CellGenix GMP SCGM, 20802-0500) supplemented with 10% heat-inactivated human AB plasma from healthy donors (Sigma, male AB, H-4522), 1% L-glutamine, 1% Pen-Strep, 1% sodium pyruvate, 1% MEM-Eagle, 1% HEPES 1 M, and 300 IU/mL recombinant human IL-2 (PeproTech).

Cell Affinity Studies. Cultured pNK cells were seeded onto the surfaces in growth medium containing <2% serum and 50 units of Il-2 and left to adhere for 3−4 h. The surfaces were then rinsed twice in PBS to remove the nonadherent cells, followed by fixing the adherent cells with 4% PFA, permeabilization with 0.5% Triton-X 100, and blocked with 5% skim milk in PBS. The actin cytoskeleton was stained with Alexa Fluor 555 phalloidin, and the nuclei were stained by mounting the samples with ProLong Gold antifade reagent containing DAPI (both from Life Technologies).

Cell Activation Studies. Cultured pNK cells were seeded as previously mentioned. The medium was supplemented with APC anti-human CD107a (1:1000 v/v) and was left to adhere for 3 h. The medium was then renewed, and the cells were placed on ice for 30 min to maximize the membrane-bound CD107a. The surfaces were then rinsed twice in PBS, fixed with 4% PFA, and then directly stained with Alexa Fluor 555 phalloidin without permeabilization to prevent damage to the cell membrane. Finally, the nuclei were stained by mounting the samples with ProLong Gold antifade reagent containing DAPI.

X-ray Photoelectron Microscopy. XPS data were collected using an X-ray photoelectron spectrometer ESCALAB 250 ultrahigh vacuum (1×10^{-9} bar) apparatus with an Al Kα X-ray source and a monochromator. The X-ray beam size was 500 μm, and the survey spectra were recorded with a pass energy (PE) of 150 eV, and high-energy resolution spectra were recorded with a PE of 20 eV. To correct for charging effects, all spectra were calibrated relative to a carbon C 1s peak positioned at 284.8 eV. The processing of the XPS results was carried out using the AVANTAGE program.

Microscopy. The characterization of the surfaces as well as NK cell adhesion and activation was performed using a Zeiss LSM880 confocal microscope and quantified using the Fiji imaging software (https://fiji.sc). Locating cells on disks was done by merging Alexa phalloidin 555 and NeutrAvidin 488 channels. The cells with cytoskeletons that did not "touch" the disks were considered out of the disks. For APC anti-CD107a, quantification of fluorescence intensity, exposure time, detector gain, and laser power were optimized once on the first sample and then locked. From the APC anti-CD107a signal, we quantified the percentage of activated cells by applying a threshold below which the cells were considered nonactivated. In addition, assuming that the degree of activation is proportional to the intensity of the APC anti-CD107a signal, the degree of NK cell activation can also be quantified.

Statistics. At least 10 fields at 20× magnification on each surface were analyzed. The data were averaged for each experiment, and the experiments were performed three times. Statistical analysis was performed by analysis of variance, and Tukey's multiple-comparison post hoc test was also performed using the Prism software (GraphPad Software Inc., USA). The results were considered to be significantly different for $p < 0.05$. *P*-values are also reported for comparisons of interest.

■ ASSOCIATED CONTENT

Supporting Information

The Supporting Information is available free of charge on the ACS Publications website at DOI: 10.1021/acsami.7b19643.

Complementary analysis by XPS, fluorescence microscopy of the functionalized surfaces, quantification of the relative surface density of moieties on bi-functional micro-arrays and *z*-stack imaging showing the location of granules relative to the surface (PDF)

■ AUTHOR INFORMATION

Corresponding Authors

*E-mail: lesaux@post.bgu.ac.il (G.L.S.).
*E-mail: marksc@bgu.ac.il (M.S.).

ORCID

Guillaume Le Saux: 0000-0003-4902-1980
Mark Schvartzman: 0000-0002-5912-525X

Author Contributions

The manuscript was written through contributions from all authors. All authors have given approval to the final version of the manuscript.

Notes

The authors declare no competing financial interest.

■ ACKNOWLEDGMENTS

This work was funded by the Multidisciplinary Research Grant—The Faculty of Health Science in Ben-Gurion University of the Negev and Israel Ministry of Science and Technology: Israel-Taiwan Collaborative grant # 3-12409. The manuscript was written through contributions from all authors.

DOI: 10.1021/acsami.7b19643
ACS Appl. Mater. Interfaces 2018, 10, 11486−11494

REFERENCES

(1) Eliceiri, B. P. Integrin and Growth Factor Receptor Crosstalk. *Circ. Res.* **2001**, *89*, 1104−1110.
(2) Ogita, H.; Takai, Y. Cross-Talk among Integrin, Cadherin, and Growth Factor Receptor: Roles of Nectin and Nectin-like Molecule. *Int. Rev. Cytol.* **2008**, *265*, 1−54.
(3) Lin, A.; Devaux, B.; Green, A.; Sagerstrom, C.; Elliott, J.; Davis, M. Expression of T Cell Antigen Receptor Heterodimers in a Lipid-Linked Form. *Science* **1990**, *249*, 677−679.
(4) Lanier, L. L. Up on the Tightrope: Natural Killer Cell Activation and Inhibition. *Nat. Immunol.* **2008**, *9*, 495−502.
(5) Pegram, H. J.; Andrews, D. M.; Smyth, M. J.; Darcy, P. K.; Kershaw, M. H. Activating and Inhibitory Receptors of Natural Killer Cells. *Immunol. Cell Biol.* **2011**, *89*, 216−224.
(6) Kruse, P. H.; Matta, J.; Ugolini, S.; Vivier, E. Natural Cytotoxicity Receptors and Their Ligands. *Immunol. Cell Biol.* **2014**, *92*, 221−229.
(7) Endt, J.; McCann, F. E.; Almeida, C. R.; Urlaub, D.; Leung, R.; Pende, D.; Davis, D. M.; Watzl, C. Inhibitory Receptor Signals Suppress Ligation-Induced Recruitment of NKG2D to GM1-Rich Membrane Domains at the Human NK Cell Immune Synapse. *J. Immunol.* **2007**, *178*, 5606−5611.
(8) Bryceson, Y. T.; Ljunggren, H.-G.; Long, E. O. Minimal Requirement for Induction of Natural Cytotoxicity and Intersection of Activation Signals by Inhibitory Receptors. *Blood* **2009**, *114*, 2657−2666.
(9) Choudhuri, K.; Parker, M.; Milicic, A.; Cole, D. K.; Shaw, M. K.; Sewell, A. K.; Stewart-Jones, G.; Dong, T.; Gould, K. G.; van der Merwe, P. A. Peptide-Major Histocompatibility Complex Dimensions Control Proximal Kinase-Phosphatase Balance during T Cell Activation. *J. Biol. Chem.* **2009**, *284*, 26096−26105.
(10) Choudhuri, K.; Wiseman, D.; Brown, M. H.; Gould, K.; van der Merwe, P. A. T-Cell Receptor Triggering Is Critically Dependent on the Dimensions of Its Peptide-MHC Ligand. *Nature* **2005**, *436*, 578−582.
(11) Rossy, J.; Owen, D. M.; Williamson, D. J.; Yang, Z.; Gaus, K. Conformational States of the Kinase Lck Regulate Clustering in Early T Cell Signaling. *Nat. Immunol.* **2012**, *14*, 82−89.
(12) Bashour, K. T.; Tsai, J.; Shen, K.; Lee, J.-H.; Sun, E.; Milone, M. C.; Dustin, M. L.; Kam, L. C. Cross Talk between CD3 and CD28 Is Spatially Modulated by Protein Lateral Mobility. *Mol. Cell. Biol.* **2014**, *34*, 955−964.
(13) Steinle, A.; Li, P.; Morris, D. L.; Groh, V.; Lanier, L. L.; Strong, R. K.; Spies, T. Interactions of Human NKG2D with Its Ligands MICA, MICB, and Homologs of the Mouse RAE-1 Protein Family. *Immunogenetics* **2001**, *53*, 279−287.
(14) Köhler, K.; Xiong, S.; Brzostek, J.; Mehrabi, M.; Eissmann, P.; Harrison, A.; Cordoba, S.-P.; Oddos, S.; Miloserdov, V.; Gould, K.; Burroughs, N. J.; van der Merwe, P. A.; Davis, D. M. Matched Sizes of Activating and Inhibitory Receptor/Ligand Pairs Are Required for Optimal Signal Integration by Human Natural Killer Cells. *PLoS One* **2010**, *5*, No. e15374.
(15) Pageon, S. V.; Cordoba, S.-P.; Owen, D. M.; Rothery, S. M.; Oszmiana, A.; Davis, D. M. Superresolution Microscopy Reveals Nanometer-Scale Reorganization of Inhibitory Natural Killer Cell Receptors upon Activation of NKG2D. *Sci. Signaling* **2013**, *6*, ra62.
(16) Rapoport, A. P.; Stadtmauer, E. A.; Binder-Scholl, G. K.; Goloubeva, O.; Vogl, D. T.; Lacey, S. F.; Badros, A. Z.; Garfall, A.; Weiss, B.; Finklestein, J.; Kulikovskaya, I.; Sinha, S. K.; Kronsberg, S.; Gupta, M.; Bond, S.; Melchiori, L.; Brewer, J. E.; Bennett, A. D.; Gerry, A. B.; Pumphrey, N. J.; Williams, D.; Tayton-Martin, H. K.; Ribeiro, L.; Holdich, T.; Yanovich, S.; Hardy, N.; Yared, J.; Kerr, N.; Philip, S.; Westphal, S.; Siegel, D. L.; Levine, B. L.; Jakobsen, B. K.; Kalos, M.; June, C. H. NY-ESO-1−specific TCR−engineered T Cells Mediate Sustained Antigen-Specific Antitumor Effects in Myeloma. *Nat. Med.* **2015**, *21*, 914−921.
(17) Grupp, S. A.; Kalos, M.; Barrett, D.; Aplenc, R.; Porter, D. L.; Rheingold, S. R.; Teachey, D. T.; Chew, A.; Hauck, B.; Wright, J. F.; Milone, M. C.; Levine, B. L.; June, C. H. Chimeric Antigen Receptor−Modified T Cells for Acute Lymphoid Leukemia. *N. Engl. J. Med.* **2013**, *368*, 1509−1518.
(18) Menon, S.; Shin, S.; Dy, G. Advances in Cancer Immunotherapy in Solid Tumors. *Cancers* **2016**, *8*, 106.
(19) Kilian, K. A.; Bugarija, B.; Lahn, B. T.; Mrksich, M. Geometric Cues for Directing the Differentiation of Mesenchymal Stem Cells. *Proc. Natl. Acad. Sci. U.S.A.* **2010**, *107*, 4872−4877.
(20) Bilem, I.; Chevallier, P.; Plawinski, L.; Sone, E. D.; Durrieu, M.-C.; Laroche, G. Interplay of Geometric Cues and RGD/BMP-2 Crosstalk in Directing Stem Cell Fate. *ACS Biomater. Sci. Eng.* **2017**, *3*, 2514−2523.
(21) Weisbecker, C. S.; Merritt, M. V.; Whitesides, G. M. Molecular Self-Assembly of Aliphatic Thiols on Gold Colloids. *Langmuir* **1996**, *12*, 3763−3772.
(22) Adden, N.; Gamble, L. J.; Castner, D. G.; Hoffmann, A.; Gross, G.; Menze, H. Phosphonic Acid Monolayers for Binding of Bioactive Molecules to Titanium Surfaces. *Langmuir* **2006**, *22*, 8197−8204.
(23) Dubacheva, G. V.; Araya-Callis, C.; Volbeda, A. G.; Fairhead, M.; Codée, J.; Howarth, M.; Richter, R. P. Controlling Multivalent Binding through Surface Chemistry: Model Study on Streptavidin. *J. Am. Chem. Soc.* **2017**, *139*, 4157−4167.
(24) Maury, P.; Escalante, M.; Péter, M.; Reinhoudt, D. N.; Subramaniam, V.; Huskens, J. Creating Nanopatterns of His-Tagged Proteins on Surfaces by Nanoimprint Lithography Using Specific NiNTA-Histidine Interactions. *Small* **2007**, *3*, 1584−1592.
(25) Burdinski, D.; Saalmink, M.; van den Berg, J. P. W. G.; van der Marel, C. Universal Ink for Microcontact Printing. *Angew. Chem., Int. Ed.* **2006**, *45*, 4355−4358.
(26) Bhat, R.; Sell, S.; Wagner, R.; Zhang, J. T.; Pan, C.; Garipcan, B.; Boland, W.; Bossert, J.; Klemm, E.; Jandt, K. D. The Janus-SAM Approach for the Flexible Functionalization of Gold and Titanium Oxide Surfaces. *Small* **2010**, *6*, 465−470.
(27) Guasch, J.; Conings, B.; Neubauer, S.; Rechenmacher, F.; Ende, K.; Rolli, C. G.; Kappel, C.; Schaufler, V.; Micoulet, A.; Kessler, H.; Boyen, H.-G.; Cavalcanti-Adam, E. A.; Spatz, J. P. Segregation Versus Colocalization: Orthogonally Functionalized Binary Micropatterned Substrates Regulate the Molecular Distribution in Focal Adhesions. *Adv. Mater.* **2015**, *27*, 3737−3747.
(28) Bilem, I.; Chevallier, P.; Plawinski, L.; Sone, E. D.; Durrieu, M. C.; Laroche, G. RGD and BMP-2 Mimetic Peptide Crosstalk Enhances Osteogenic Commitment of Human Bone Marrow Stem Cells. *Acta Biomater.* **2016**, *36*, 132−142.
(29) Ghaemi, S. R.; Delalat, B.; Cetó, X.; Harding, F. J.; Tuke, J.; Voelcker, N. H. Synergistic Influence of Collagen I and BMP 2 Drives Osteogenic Differentiation of Mesenchymal Stem Cells: A Cell Microarray Analysis. *Acta Biomater.* **2016**, *34*, 41−52.
(30) Hermanson, G. T. Bioconjugate Techniques, 3rd ed.; Elsevier, 2013.
(31) Mani, G.; Johnson, D. M.; Marton, D.; Feldman, M. D.; Patel, D.; Ayon, A. A.; Agrawal, C. M. Drug Delivery from Gold and Titanium Surfaces Using Self-Assembled Monolayers. *Biomaterials* **2008**, *29*, 4561−4573.
(32) Paniagua, S. A.; Hotchkiss, P. J.; Jones, S. C.; Marder, S. R.; Mudalige, A.; Marrikar, F. S.; Pemberton, J. E.; Armstrong, N. R. Phosphonic Acid Modification of Indium-Tin Oxide Electrodes: Combined XPS/UPS/Contact Angle Studies. *J. Phys. Chem. C* **2008**, *112*, 7809−7817.
(33) Kosian, M.; Smulders, M. M. J.; Zuilhof, H. Structure and Long-Term Stability of Alkylphosphonic Acid Monolayers on SS316L Stainless Steel. *Langmuir* **2016**, *32*, 1047−1057.
(34) Bauer, S.; Groh, V.; Wu, J.; Steinle, A.; Phillips, J. H.; Lanier, L. L.; Spies, T. Activation of NK Cells and T Cells by NKG2D, a Receptor for Stress-Inducible MICA. *Science* **1999**, *285*, 727−729.
(35) Ferlazzo, G.; Tsang, M. L.; Moretta, L.; Melioli, G.; Steinman, R. M.; Münz, C. Human Dendritic Cells Activate Resting Natural Killer (NK) Cells and Are Recognized via the NKp30 Receptor by Activated NK Cells. *J. Exp. Med.* **2002**, *195*, 343−351.
(36) Delcassian, D.; Depoil, D.; Rudnicka, D.; Liu, M.; Davis, D. M.; Dustin, M. L.; Dunlop, I. E. Nanoscale Ligand Spacing Influences

DOI: 10.1021/acsami.7b19643
ACS Appl. Mater. Interfaces 2018, 10, 11486−11494

Receptor Triggering in T Cells and NK Cells. *Nano Lett.* **2013**, *13*, 5608−5614.
(37) Timonen, T. Natural Killer Cells: Endothelial Interactions, Migration, and Target Cell Recognition. *J. Leukocyte Biol.* **1997**, *62*, 693−701.
(38) Serrano-Pertierra, E.; Cernuda-Morollón, E.; Brdička, T.; Hoøejši, V.; López-Larrea, C. L-Plastin Is Involved in NKG2D Recruitment into Lipid Rafts and NKG2D-Mediated NK Cell Migration. *J. Leukocyte Biol.* **2014**, *96*, 437−445.
(39) Walzer, T.; Vivier, E. G-Protein-Coupled Receptors in Control of Natural Killer Cell Migration. *Trends Immunol.* **2011**, *32*, 486−492.
(40) Alter, G.; Malenfant, J. M.; Altfeld, M. CD107a as a Functional Marker for the Identification of Natural Killer Cell Activity. *J. Immunol. Methods* **2004**, *294*, 15−22.
(41) Orange, J. S. Formation and Function of the Lytic NK-Cell Immunological Synapse. *Nat. Rev. Immunol.* **2008**, *8*, 713−725.
(42) Costello, R. T.; Boehrer, A.; Sanchez, C.; Mercier, D.; Baier, C.; Le Treut, T.; Sébahoun, G. Differential Expression of Natural Killer Cell Activating Receptors in Blood versus Bone Marrow in Patients with Monoclonal Gammopathy. *Immunology* **2013**, *139*, 338−341.
(43) Cao, B.; Peng, Y.; Liu, X.; Ding, J. Effects of Functional Groups of Materials on Nonspecific Adhesion and Chondrogenic Induction of Mesenchymal Stem Cells on Free and Micropatterned Surfaces. *ACS Appl. Mater. Interfaces* **2017**, *9*, 23574−23585.
(44) Ye, K.; Cao, L.; Li, S.; Yu, L.; Ding, J. Interplay of Matrix Stiffness and Cell−Cell Contact in Regulating Differentiation of Stem Cells. *ACS Appl. Mater. Interfaces* **2016**, *8*, 21903−21913.
(45) Yao, X.; Peng, R.; Ding, J. Cell-Material Interactions Revealed Via Material Techniques of Surface Patterning. *Adv. Mater.* **2013**, *25*, 5257−5286.
(46) Arnold, M.; Cavalcanti-Adam, E. A.; Glass, R.; Blümmel, J.; Eck, W.; Kantlehner, M.; Kessler, H.; Spatz, J. P. Activation of Integrin Function by Nanopatterned Adhesive Interfaces. *ChemPhysChem* **2004**, *5*, 383−388.
(47) Sweetman, M. J.; Ronci, M.; Ghaemi, S. R.; Craig, J. E.; Voelcker, N. H. Porous Silicon Films Micropatterned with Bioelements as Supports for Mammalian Cells. *Adv. Funct. Mater.* **2012**, *22*, 1158−1166.
(48) Dalby, M. J.; Gadegaard, N.; Tare, R.; Andar, A.; Riehle, M. O.; Herzyk, P.; Wilkinson, C. D. W.; Oreffo, R. O. C. The Control of Human Mesenchymal Cell Differentiation Using Nanoscale Symmetry and Disorder. *Nat. Mater.* **2007**, *6*, 997−1003.

DOI: 10.1021/acsami.7b19643
ACS Appl. Mater. Interfaces 2018, 10, 11486−11494